*IMA Journal of Numerical Analysis* (2007) Page 1 of 25
doi: 10.1093/imanum/dri017

# Locality properties of radial basis function expansion coefficients for equispaced interpolation

BENGT FORNBERG
*Department of Applied Mathematics, University of Colorado*
*Boulder, CO 80309, USA (fornberg@colorado.edu)*

NATASHA FLYER
*Institute for Mathematics Applied to the Geosciences, National Center for Atmospheric Research*
*Boulder, CO 80307, USA (flyer@ucar.edu)*

SUSAN HOVDE AND CÉCILE PIRET
*Same address as first author, (hovde@colorado.edu), (piret@colorado.edu)*

[Submitted on 14 September 2006; Revised April 25 2007]

Many types of radial basis functions (RBFs) are global, in terms of having large magnitude across the entire domain. Yet, in contrast, for example, with expansions in orthogonal polynomials, RBF expansions exhibit a strong property of locality with regard to their coefficients. That is, changing a single data value mainly affects the coefficients of the RBFs which are centered in the immediate vicinity of that data location. This locality feature can be advantageous in the development of fast and well conditioned iterative RBF algorithms. With this motivation, we employ here both analytical and numerical techniques to derive the decay rates of the expansion coefficients for cardinal data, in both 1-D and 2-D. Furthermore, we explore how these rates vary in the interesting high-accuracy limit of increasingly flat RBFs.

*Keywords*: Radial basis functions, RBF, cardinal interpolation

## 1. Introduction

Radial basis functions (RBF) provide a well established approach to the task of interpolating scattered data in multiple dimensions. With a *radial function* $\phi(r)$ and with data values $f_k$ given at locations $\underline{x}_k$, $k = 1, 2, \ldots, n$, the function

$$s(\underline{x}) = \sum_{k=1}^{n} \lambda_k \, \phi(||\underline{x} - \underline{x}_k||), \tag{1.1}$$

where $\|\cdot\|$ denotes the standard Euclidean norm, interpolates the data if we choose the expansion coefficients $\lambda_k$ in such a way that $s(\underline{x}_k) = f_k$, $k = 1, 2, \ldots, n$. During the last decade, it has become increasingly well recognized that interpolants of this form – when $\phi(r)$ is infinitely differentiable – provide a natural generalization, to arbitrary geometries, of pseudospectral (PS) methods (Driscoll & Fornberg (2002), Fornberg (1996), Fornberg et al. (2004)) for solving PDEs. These differentiable RBFs can be scaled by means of a *shape parameter*, in this paper denoted by $\varepsilon$, so that we frequently write $\phi(r;\varepsilon)$. It turns out that *every* classical PS method (Fourier, Chebyshev, etc.) arises as a special case of RBF interpolation Driscoll & Fornberg (2002), Fornberg et al. (2004) in the limit as $\phi(r;\varepsilon)$ becomes flat (i.e. as $\varepsilon \to 0$).

Successive basis functions in classical basis sets (such as Fourier and Chebyshev sets) are global

and increasingly oscillatory. Altering a single data value will change all expansion coefficients by roughly the same amount - i.e. there is no concept of 'locality' in the resulting expansion. The RBF basis is fundamentally different in a number of ways. In return for giving up the orthogonality of the basis functions, unconditional non-singularity is gained with scattered node locations for many cases of radial functions $\phi(r)$. Although the basis functions typically are global (e.g. the popular choice of $\phi(r) = \sqrt{1+(\varepsilon r)^2}$ ), the interpolant will nevertheless feature strong locality in the sense that changing the data at one point will mainly influence expansion coefficients of basis functions centered in its immediate vicinity. If the locality was perfect (only one coefficient being affected), the linear system to solve would be diagonal, i.e. perfectly conditioned. Since lack of locality can cause ill-conditioning, a study of locality will give insights into how different radial functions compare in this regard. The degree of locality enters also in the convergence rates of some iterative procedures for rapid computation of the expansion coefficients (Buhmann (2003) Chapter 7, Faul & Powell (2000)).

The concept of locality associated with RBF interpolation on equispaced lattices was first addressed by Buhmann (Buhmann (1988), Buhmann (1993), Buhmann & Powell (1990)), who studied the behavior of the RBF interpolant to cardinal data (a single data value being one and all others equal to zero) in the asymptotic limit as $||\underline{x}|| \to \infty$ along a coordinate axis. While our analysis also considers cardinal data, we instead concentrate on studying the behavior of the resulting RBF expansion coefficients, $\lambda_k$, for increasing $|k|$. It should be noted that there is a striking similarity between the integrals that describe the coefficients and those that represent the interpolant for cardinal data. This similarity is discussed and developed further in the context of exploring Gibbs phenomena for RBFs Fornberg & Flyer (in press). In cases where closed form expressions for the integrals that represent the coefficients are not possible (which is the usual circumstance), we present an asymptotic approach using contour integration that captures the behavior of $\lambda_k$ for both small and large $k$, noting very different trends in each case. It is the former case ($k$ small) that almost always determines the localization property of the RBF expansion (thin plate splines being the exception). Also not previously observed in the literature is that the decay rate of $\lambda_k$ for 2-D interpolation is dependent not only on radial distance but also on the angle in coefficient space (and likewise in higher dimensions). In addition, our study also illuminates the dependence of the decay rate on the shape parameter $\varepsilon$ for infinitely smooth RBFs.

RBFs are mainly of interest when the data locations are scattered. Since effective theoretical analysis for such cases does not appear to be practical, this study is focused on cases with node points on equispaced lattices (in one and more dimensions). In a follow-up studies, we will consider scattered nodes, in particular when distributed over the surface of a sphere. Preliminary numerical results show trends which qualitatively match those observed in the current paper.

The paper is organized as follows. Section 2 focuses on closed-form expressions for the RBF expansion coefficients in one or more dimensions using Fourier analysis. Explicit formulas are obtained for a few RBF cases, exhibiting a variety of decay behaviors for the expansion coefficients. However, such explicit expressions are rare even in 1-D, making it necessary to obtain asymptotic estimates. It is shown in Section 3 how contour integration offers a particularly effective way to estimate the size of the cardinal expansion coefficients in 1-D for both small and large $k$. These observations are summarized in Section 4, with a discussion of the situation in higher dimensions given in Section 5. Section 6, with a summary of observations, is followed by Appendix A proving non-singularity of a less commonly used type of radial function. Appendix B presents the asymptotic analysis for the generalized multiquadric RBF.

## 2. Closed form expressions for cardinal coefficients

### 2.1 *Basic formulas*

We consider first the situation in 1-D and base the analysis in this section on the assumption of a constant node spacing $h = 1$. The radial function $\phi(r)$ takes, at the lattice points $x_k = k \in Z$, the values $\phi(k)$. The cardinal expansion coefficients $\lambda_k,\ k \in Z$, will then satisfy

$$\sum_{k=-\infty}^{\infty} \lambda_k\, \phi(n-k) = \begin{cases} 1 & n = 0 \\ 0 & n \neq 0,\ n \in Z \end{cases} . \tag{2.1}$$

In terms of the $2\pi$-periodic functions

$$\Lambda(\xi) = \sum_{k=-\infty}^{\infty} \lambda_k\, e^{ik\xi}$$

and

$$\Xi(\xi) = \sum_{k=-\infty}^{\infty} \phi(k)\, e^{ik\xi},$$

the convolution in (2.1) can be expressed as

$$\Lambda(\xi) \cdot \Xi(\xi) = 1.$$

We adhere to the convention of defining the Fourier transform through the relations $f(x) = \frac{1}{\sqrt{2\pi}} \int_{-\infty}^{\infty} \widehat{f}(\omega)\, e^{i\omega x} d\omega$, $\widehat{f}(\omega) = \frac{1}{\sqrt{2\pi}} \int_{-\infty}^{\infty} f(x)\, e^{-i\omega x} dx$. Furthermore, radial functions are symmetric, i.e. $\phi(r) = \phi(-r)$ implying $\lambda_k = \lambda_{-k}$. It follows then from the Poisson summation formula that

$$\Xi(\xi) = \sqrt{2\pi} \sum_{k=-\infty}^{\infty} \widehat{\phi}(\xi + 2\pi k), \tag{2.2}$$

and we obtain the cardinal expansion coefficients explicitly (as has been observed earlier, e.g. Buhmann & Powell (1990), Buhmann (2003)) as

$$\lambda_k = \frac{1}{(2\pi)^{3/2}} \int_0^{2\pi} \frac{e^{ik\xi}}{\sum\limits_{j=-\infty}^{\infty} \widehat{\phi}(|\xi + 2\pi j|)} d\xi. \tag{2.3}$$

In cases where the regular Fourier transform for $\phi(r)$ fails to exist, the generalized Fourier transform can be used (e.g. Arsac (1966), Jones (1966), Lighthill (1958)).

We can note that the expression for the interpolant becomes

$$s(x) = \frac{1}{2\pi} \int_{-\infty}^{\infty} \frac{\widehat{\phi}(\xi) e^{ix\xi}}{\sum\limits_{j=-\infty}^{\infty} \widehat{\phi}(|\xi + 2\pi j|)} d\xi. \tag{2.4}$$

This differs from (2.3) mainly in two ways: 1) the factor of $\widehat{\phi}(\xi)$ in the numerator and 2) the integral is taken over $(-\infty, \infty)$. As a result, there is a close relationship between the expansion coefficients, $\lambda_k$, and the interpolant, $s(x)$. Fuller exploration of this relationship will be postponed to a follow-up paper, as it would distract from our current theme.

For cardinal expansions in $n$-D, (2.3) generalizes to

$$\lambda_{k_1,\ldots,k_n} = \frac{1}{(2\pi)^{(3n)/2}} \int_0^{2\pi} \cdots \int_0^{2\pi} \frac{e^{i\underline{k}\cdot\underline{\xi}}}{\sum\limits_{j_1=-\infty}^{\infty} \cdots \sum\limits_{j_n=-\infty}^{\infty} \widehat{\phi}(\|\underline{\xi}+2\pi\underline{j}\|)} d\underline{\xi}. \tag{2.5}$$

Table 1 lists some examples of radial functions $\phi(r)$ and their (generalized) Fourier transforms. Non-singularity of the RBF interpolant in the SH case (for scattered data in $n$ dimensions) was first shown in Gneiting (1997). A new shorter proof is furnished in Appendix A.

The multidimensional Fourier transforms in Table 1 are most easily carried out by means of the Hankel relation

$$\begin{aligned} \widehat{\phi}(\|\underline{\xi}\|) &= (2\pi)^{-n/2} \int_{-\infty}^{\infty} \cdots \int_{-\infty}^{\infty} \phi(\|\underline{x}\|)\, e^{-i\underline{\xi}\cdot\underline{x}} d\underline{x} \\ &= \frac{1}{\rho^{(n-2)/2}} \int_0^{\infty} \phi(r)\, r^{n/2}\, J_{(n-2)/2}(r\rho) dr, \end{aligned} \tag{2.6}$$

where $\rho^2 = \xi_1^2 + \xi_2^2 + \ldots + \xi_n^2$ and $r^2 = x_1^2 + x_2^2 + \ldots + x_n^2$.

With the use of some Bessel function identities, (2.6) can alternatively be expressed as follows:
$n = 2m+1$ odd:

$$\widehat{\phi}(\rho) = (-2)^m \sqrt{\frac{2}{\pi}} \frac{d^m}{d(\rho^2)^m} \int_0^{\infty} \phi(r) \cos(\rho r) dr \tag{2.7}$$

$n = 2m+2$ even:

$$\widehat{\phi}(\rho) = (-2)^m \frac{d^m}{d(\rho^2)^m} \int_0^{\infty} \phi(r)\, r\, J_0(\rho r) dr. \tag{2.8}$$

### 2.2 *Some 1-D special cases with simple explicit formulas*

In rare cases, both the infinite sum and the integral in (2.3) can be obtained in closed form. However, these examples are exceptions rather than the rule. They highlight the need for a more general approach that can provide approximations on how the coefficients decay away from $k = 0$ as $|k|$ increases for arbitrary radial functions.

2.2.1 *Cubics* For cubics $\phi(r) = |r|^3$, we obtain (as was noted in Fornberg et al. (2002))

$$\lambda_0 = -4 + 3\sqrt{3}, \;\; \lambda_1 = \frac{19}{2} - 6\sqrt{3} \;\text{ and }\; \lambda_k = \frac{(-1)^k 3\sqrt{3}}{(2+\sqrt{3})^k},\; k \geqslant 2. \tag{2.9}$$

(recalling that $\lambda_{-k} = \lambda_k$).

2.2.2 *IQ* In this case, the sum (but not the integral) can be evaluated in closed form. As was also noted in Fornberg et al. (2002), we then get

$$\lambda_k = \frac{(-1)^k \varepsilon\, \sinh(\frac{\pi}{\varepsilon})}{\pi^2} \int_0^{\pi} \frac{\cos k\xi}{\cosh(\xi/\varepsilon)} d\xi, \;\; k \in Z. \tag{2.10}$$

| **Type of radial function** | | | **Fourier transform** $\widehat{\phi}(\rho)$ in $n$-D |
|---|---|---|---|
| **Piecewise smooth** | | | |
| MN | monomial | $\lvert r\rvert^{2j+1}$ | $\frac{(-1)^{j+1}2^{2j+\frac{n}{2}+1}(j+\frac{1}{2})\Gamma\left(j+\frac{1}{2}\right)\Gamma\left(j+\frac{n+1}{2}\right)}{\pi}\frac{1}{\lvert\rho\rvert^{2j+n+1}}$ |
| TPS | thin plate spline | $\lvert r\rvert^{2j}\ln\lvert r\rvert$ | $(-1)^{j+1}2^{2j+\frac{n}{2}-1}j!\,\Gamma\left(j+\frac{n}{2}\right)\frac{1}{\lvert\rho\rvert^{2j+n}}$ |
| **Infinitely smooth** | | | |
| GMQ | generalized MQ | $(1+(\varepsilon r)^2)^{\beta}$ | $\frac{2^{\beta+1}}{\Gamma(-\beta)\varepsilon^{n/2-\beta}}\frac{K_{n/2+\beta}\left(\frac{\lvert\rho\rvert}{\varepsilon}\right)}{\lvert\rho\rvert^{n/2+\beta}}$ |
| | MQ | $\sqrt{1+(\varepsilon r)^2}$ | $-\frac{\sqrt{2}}{\sqrt{\pi}\,\varepsilon^{\frac{n-1}{2}}}\frac{K_{\frac{n+1}{2}}\left(\frac{\lvert\rho\rvert}{\varepsilon}\right)}{\lvert\rho\rvert^{\frac{n+1}{2}}}$ |
| | IMQ | $\frac{1}{\sqrt{1+(\varepsilon r)^2}}$ | $\frac{\sqrt{2}}{\sqrt{\pi}\,\varepsilon^{\frac{n+1}{2}}}\frac{K_{\frac{n-1}{2}}\left(\frac{\lvert\rho\rvert}{\varepsilon}\right)}{\lvert\rho\rvert^{\frac{n-1}{2}}}$ |
| | IQ | $\frac{1}{1+(\varepsilon r)^2}$ | $\frac{1}{\varepsilon^{\frac{n}{2}+1}}\frac{K_{\frac{n}{2}-1}\left(\frac{\lvert\rho\rvert}{\varepsilon}\right)}{\lvert\rho\rvert^{\frac{n}{2}-1}}$ |
| GA | Gaussian | $e^{-(\varepsilon r)^2}$ | $\frac{e^{-\rho^2/(4\varepsilon^2)}}{(\sqrt{2}\varepsilon)^n}$ |
| SH | sech | $\operatorname{sech}\varepsilon r$ | $\frac{\pi^{\frac{n}{2}}}{(2\rho)^{\frac{n}{2}-1}\varepsilon^{\frac{n}{2}+1}}\sum_{k=0}^{\infty}(-1)^k(2k+1)^{\frac{n}{2}}K_{1-\frac{n}{2}}\left(\frac{\pi\rho}{2\varepsilon}\left(k+\frac{1}{2}\right)\right)$ |
| BSL | Bessel | $\frac{J_{\frac{d}{2}-1}(\varepsilon r)}{(\varepsilon r)^{\frac{d}{2}-1}}$ | $\begin{cases}\frac{\left(1-\frac{\lvert\rho\rvert^2}{\varepsilon^2}\right)^{\frac{d-n}{2}-1}}{\varepsilon^n 2^{\frac{d}{2}-1}\Gamma\left(\frac{d-n}{2}\right)\pi^{\frac{n}{2}}}, & \text{if } \lvert\rho\rvert\leqslant\varepsilon\\ 0, & \text{if } \lvert\rho\rvert>\varepsilon\end{cases}$ |

Table 1. Regular or generalized Fourier transforms for some cases of radial functions

2.2.3 *GA* The exact result can be written as a ratio of two sums

$$\lambda_k = \frac{e^{(\varepsilon k)^2}}{2} \cdot \frac{\sum_{j=k}^{\infty} (-1)^j \, e^{-\varepsilon^2 (j+\frac{1}{2})^2}}{\sum_{j=0}^{\infty} (-1)^j (j+\frac{1}{2}) \, e^{-\varepsilon^2 (j+\frac{1}{2})^2}}, \;\; k \in Z. \tag{2.11}$$

This is most easily verified by substituting (2.11) into (2.1), noting that the denominator in (2.11) does not depend on $k$, and switching the order in the resulting double sum. A way to arrive at (2.11) (and also (2.12) below) is outlined in Section 3.4.

2.2.4 *SH* The result becomes particularly simple in this case. We find

$$\lambda_k = \frac{1}{\sum_{j=-\infty}^{\infty} (-1)^j \mathrm{sech}^2(\varepsilon j)} (-1)^k \mathrm{sech}(\varepsilon k), \;\; k \in Z. \tag{2.12}$$

In the case that $\varepsilon$ is small, the sum can be evaluated very fast by means of either of the identities

$$\begin{aligned} \sum_{j=-\infty}^{\infty} (-1)^j \mathrm{sech}^2(\varepsilon j) &= \frac{4\pi^2}{\varepsilon^2} \sum_{j=0}^{\infty} (j+\tfrac{1}{2}) \mathrm{csch}\left(\tfrac{\pi^2}{\varepsilon}(j+\tfrac{1}{2})\right) \\ &= \frac{2\pi^2}{\varepsilon^2} \sum_{j=0}^{\infty} \frac{\coth\left(\tfrac{\pi^2}{\varepsilon}(j+\tfrac{1}{2})\right)}{\sinh\left(\tfrac{\pi^2}{\varepsilon}(j+\tfrac{1}{2})\right)} \end{aligned}$$

## 3. Asymptotic analysis in 1-D by means of contour integration

We describe this approach first in the case of MQ and apply then the same methodology to other cases of radial functions.

### 3.1 *MQ*

The radial function is in this case $\phi(r) = \sqrt{1+(\varepsilon r)^2}$. For algebraic simplicity, we assume $\varepsilon = 1$ (but comment on other choices below). From (2.3) follows

$$\lambda_k = -\frac{1}{4\pi} \int_0^{2\pi} h(\xi) \, e^{ik\xi} d\xi$$

where

$$h(\xi) = \frac{1}{\sum_{j=-\infty}^{\infty} \frac{K_1(|2\pi j+\xi|)}{|2\pi j+\xi|}} \, .$$

The function $h(\xi)$ is $2\pi$-periodic and can, over $[0, 2\pi]$, be written (without taking magnitudes) as

$$h(\xi) = \frac{1}{\sum_{j=0}^{\infty} \frac{K_1(2\pi j+\xi)}{2\pi j+\xi} + \sum_{j=1}^{\infty} \frac{K_1(2\pi j-\xi)}{2\pi j-\xi}}. \tag{3.1}$$

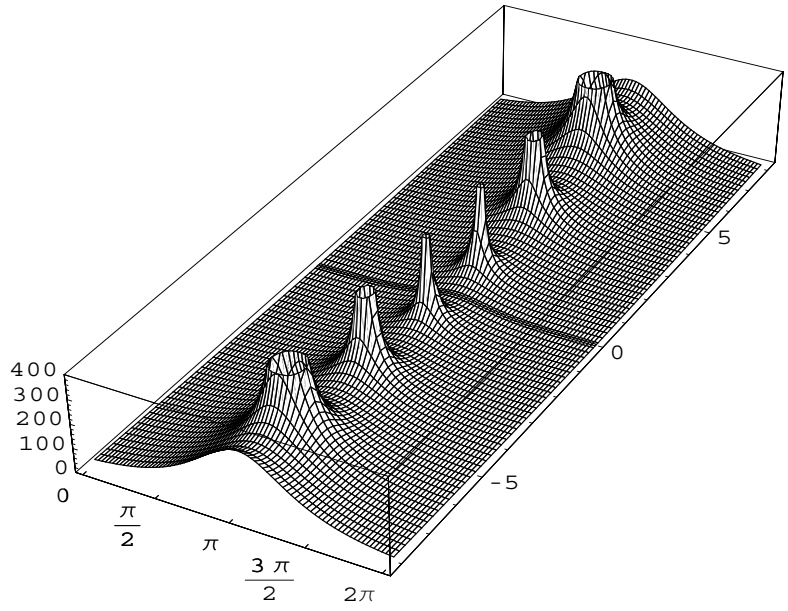


FIG. 1. Magnitude of $h(\xi)$, as given by (3.1), over the domain $0 \leqslant \mathrm{Re}\,\xi \leqslant 2\pi$, $-8 \leqslant \mathrm{Im}\,\xi \leqslant 8$.

In this form, $h(\xi)$ can be extended as a single-valued analytic function throughout the strip $0 \leqslant \mathrm{Re}\,\xi \leqslant 2\pi$. Figure 1 illustrates the magnitude of this function, and Figure 2 shows its schematic character.

We change the integration path, as is indicated in Figure 2, and note that the two leading contributions to the integral as $k$ increases will come from (i) the first pole only and (ii) from the non-cancelling contributions in the vicinity of the branch points at $\xi = 0$ and $\xi = 2\pi$. Each type of singularity contributes a different type of decay behavior to the asymptotic approximation of $\lambda_k$ for increasing $k$, as noted below.

- Contribution from the pole singularity

  Along the line $\xi = \pi + i\,t$, the function $h(\xi)$ is purely real and $1/h(\xi)$ features decaying oscillations whose roots mark the pole locations. The first pole appears near $\pi + 1.04\,i$ and has a residue of approximately $-34.6$, contributing a term of $17.3\,(-1)^{k+1}\,e^{-1.04\,k}$ to $\lambda_k$. The second pole at $t \approx 3.42$ would give a contribution of $O(e^{-3.42\,k})$, negligible compared to that of the first pole with further poles giving even smaller contributions.

- Contribution from the branch points

  The singularity of $h(\xi)$ around the origin comes from one term only in the denominator of (3.1), that is $\frac{\xi}{K_1(\xi)} = \xi^2 + (\frac{1}{4} - \frac{\gamma}{2} + \frac{\ln 2}{2} - \frac{\ln \xi}{2})\xi^4 + \ldots$ The branch singularity is of the form $-\frac{1}{2}\xi^4 \ln \xi =$

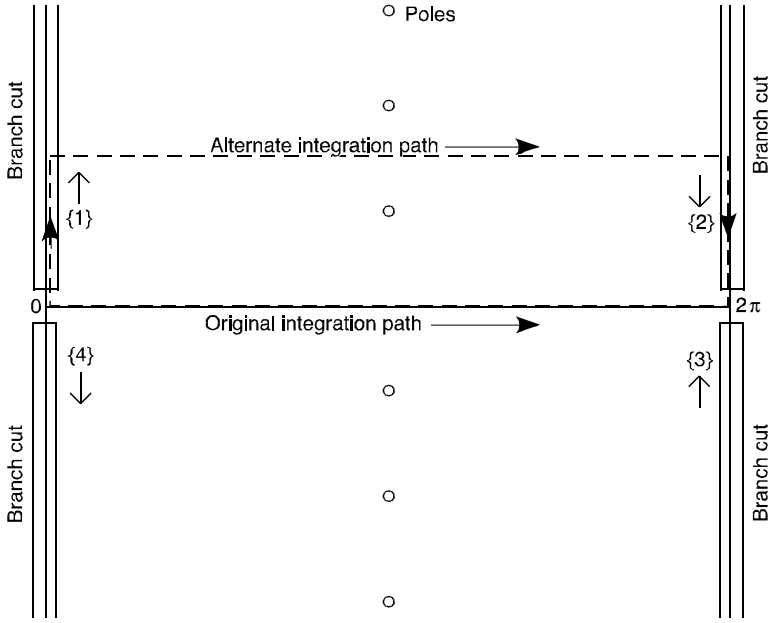


FIG. 2. Character of the function $h(\xi)$ in the complex plane. The original and the modified integration paths are shown. The additional paths marked $\{1\}$, $\{2\}$, $\{3\}$, and $\{4\}$ enter in the discussion in Appendix B.

$-\frac{1}{2}\xi^4(\ln|\xi|+i\arg\xi)$ (and similarly around $\xi=2\pi$). What does not cancel between the two sides but instead adds up (hence an extra factor of 2) amounts to $2(-\frac{1}{4\pi})\int_0^{i\cdot\{\text{some }\delta>0\}}(-\frac{1}{2})\xi^4 i\,\frac{\pi}{2}e^{-ik\xi}\,d\xi$. Letting $\xi=it$ and noting that, as $k\to\infty$, we can change the upper integration limit to infinity, this simplifies to $-\frac{1}{8}\int_0^\infty t^4e^{-kt}dt=-\frac{3}{k^5}$.

Combing these contributions gives the asymptotic approximation to $\lambda_k$ for increasing $k$:

$$\lambda_k \quad \approx \underbrace{(-1)^{k+1}\,17.3\,e^{-1.04\,k}+\ldots}_{\text{exponential part}} \quad \underbrace{-\frac{3}{k^5}+\ldots}_{\text{algebraic part}} \tag{3.2}$$

Figure 3 compares, using log-linear and log-log scales, the true values for $|\lambda_k|$ (as calculated with an accurate direct numerical approach) with the 2-term approximation in (3.2). The agreement is seen to be near-perfect. The same procedure can be carried through for any value of the shape parameter $\varepsilon$. Corresponding results for $\varepsilon=0.1$ and in the limit as $\varepsilon\to 0$ are included in Table 2.

We describe next, in more abbreviated form, the remaining cases of smooth radial functions.

### 3.2 *IQ*

Proceeding in a manner analogous to the MQ case, we find that, for general $\varepsilon$,

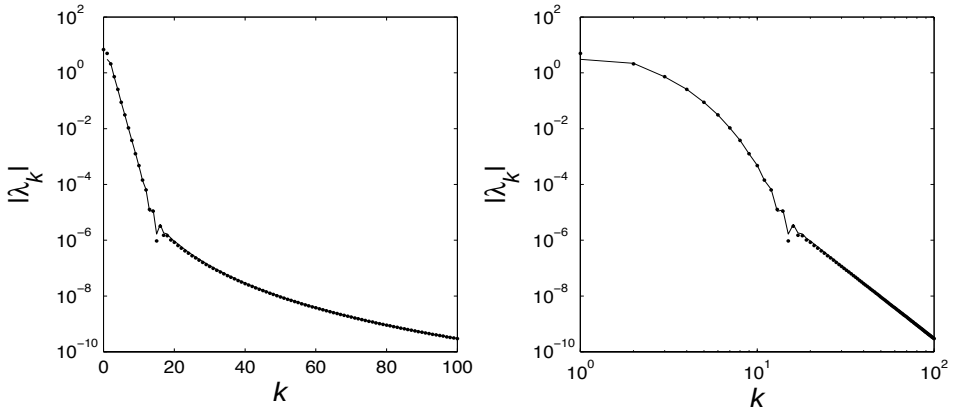


FIG. 3. Comparison between correct values of $|\lambda_k|$ for MQ in 1-D, $\varepsilon = 1$ (dots) and the 2-term asymptotic formula (3.2) (solid line). The subplot to the left is log-linear and the one to the right is log-log.

$$\lambda_k \approx \frac{(-1)^k \varepsilon^2 \sinh(\frac{\pi}{\varepsilon})}{2\pi \cosh(\frac{k\pi\varepsilon}{2})} - \frac{\tanh(\frac{\pi}{\varepsilon})^2}{\pi^2} \frac{1}{k^2}. \tag{3.3}$$

Figure 3.4 compares this approximation with an explicit computation of the $\lambda_k$. Panels (a) and (b) depict, respectively, as a function of both $k$ and $\varepsilon$, the exponential and algebraic decay surfaces corresponding to the first and second terms of (3.3). Panel (c) shows the union of these surfaces, which compares favorably with (d), the actual expansion coefficients when computed directly.

### 3.3 *GMQ*

The generalized multiquadric RBF is $\phi(r) = (1 + (\varepsilon r)^2)^\beta$. Since the analysis is very similar to the MQ case, it is given in Appendix B . Figure 5 shows, for $\varepsilon = 1$, $\log|\lambda_k|$ as a function of $\beta$ and $k$. Note the sharp dips in the algebraic decay regime at positive half integer values of $\beta$. There are no analogous features in the exponential decay regime. In both regimes the expansion coefficients approach infinity at nonnegative integer values of $\beta$.

The exponential decay of the GMQ RBF is given by the single equation (B.2), while a collection of equations, (B.5), (B.6), (B.7), (B.8), and (B.9), is needed to describe the algebraic decay, each equation corresponding to a different set of $\beta$ values. Positive half-integer values of $\beta$ are optimal in that they result in logarithmic branch points rather than algebraic, leading to much more rapid decay than achieved by other positive values (Figure 5). Indeed, judging from equation (B.5), it would seem that larger positive half-integer values would be better than smaller ones. However, in practice, to generate an interpolant to a finite number of scattered data points, a linear system is solved in order to determine the expansion coefficients $\lambda_k$, and this system becomes markedly more ill-conditioned as $\beta$ increases, in spite of the enhanced locality. That is, there is a trade-off between locality and conditioning. In this regard, $\beta = \frac{1}{2}$ is a good compromise, consistent with the reputation of the MQ RBF as being particularly useful.

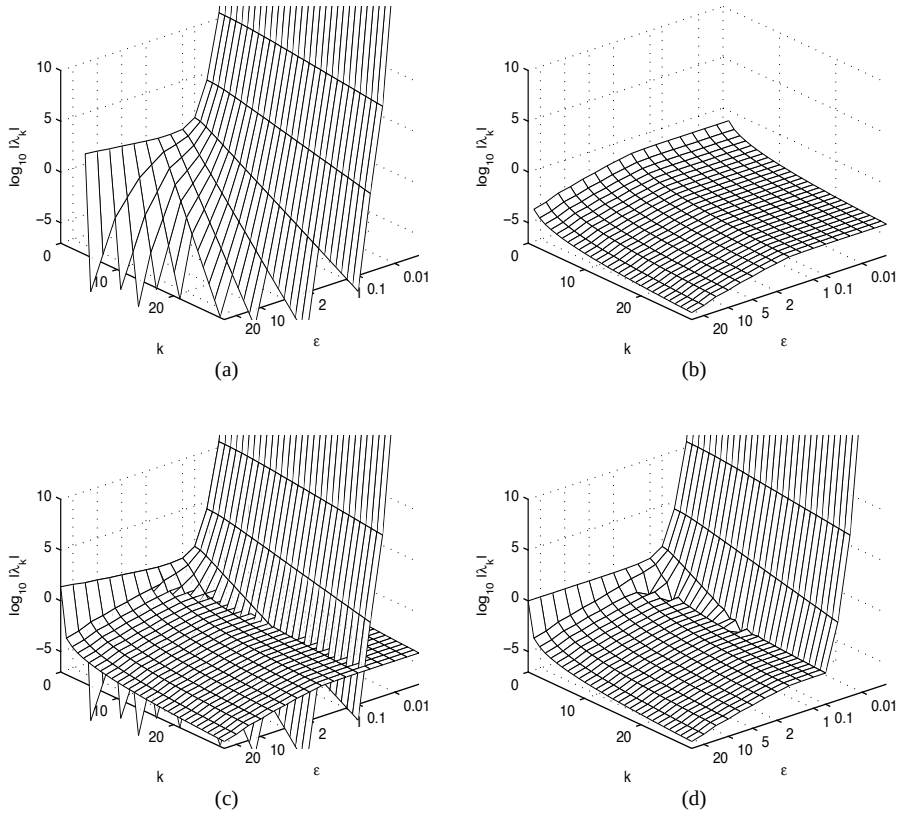


FIG. 4. Comparison of approximate and actual surfaces illustrating the decay of IQ expansion coefficients for 1-D equispaced, cardinal data. (a), the exponential decay (first term of (3.3)). (b), the algebraic decay (second term of (3.3)). (c), combination of (a) and (b). (d), actual expansion coefficients, computed explicitly. Note how well (c) approximates (d).

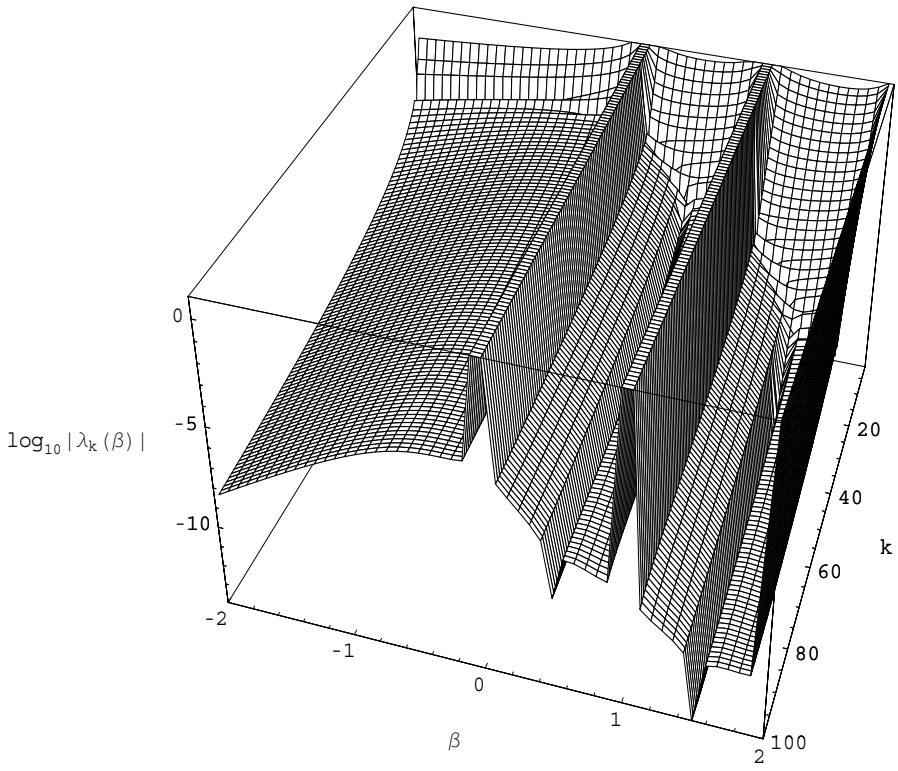


FIG. 5. Plot of log of the absolute expansion coefficients as a function of $\beta$ and $k$ and unit shape parameter. The values tend to infinity at nonnegative integers and exhibit pronounced dips in the algebraic decay at positive half-integers.

### 3.4 *GA and SH*

In these cases, there are no branch cuts, and both the locations and residues of the poles of $h(\xi)$ can be written down explicitly. The first pole provides the leading asymptotic term. The steps in arriving at (2.11) and (2.12) include moving the integration path increasingly high up in the complex plane. In the case of (2.11), the result can be further simplified by means of the relation

$$\xi(x) = \frac{1}{x^{3/2}}\,\xi(\frac{1}{x}). \tag{3.4}$$

for the function

$$\xi(x) = \sum_{j=0}^{\infty} (-1)^j (j+\tfrac{1}{2})\, e^{-\pi(j+\frac{1}{2})^2 x}. \tag{3.5}$$

### 3.5 *BSL*

The oscillatory Bessel RBF, $\phi(r) = J_{\frac{d}{2}-1}(\varepsilon r)/(\varepsilon r)^{\frac{d}{2}-1}$, gives non-singular interpolants if $d \geqslant n$, where $d$ is an integer and $n$ is the dimension of the space Fornberg et al. (2006). These are included in this study mainly to illustrate the unusual locality properties of their expansion coefficients $\lambda_k$. The BSL RBFs are different from other RBFs in that their Fourier transforms have compact support, being non-zero only on the interval $[-\varepsilon, \varepsilon]$ in 1-D (see Flyer (2006)). This implies that for $\varepsilon < \pi$, the Poisson sum $\Xi(\xi)$ in equation (2.2) will be zero over a portion of the interval $[-\pi, \pi]$, resulting in a divergent integral for $\lambda_k$ in (2.3). In such a case the coefficients $\lambda_k$ become extremely large and essentially lack locality (as seen in the top left diagram of Figure 6).

On the other hand, if $\varepsilon > \pi$ the Poisson sum (2.2) is everywhere positive. Equation (2.3) applies and the coefficients $\lambda_k$ exhibit locality. For these values of $\varepsilon$, $\Xi(\xi)$ (and therefore $1/\Xi(\xi)$) will always have two discontinuities in some derivative on the interval $[-\pi, \pi]$ due to the character of the Fourier transform and the $2\pi$ periodicity of the Poisson sum. This will lead to an algebraic decay rate for $\lambda_k$ of the type $O(1/k^{(d-1)/2})$. The preceding schematic discussion is illustrated in Figure 6.

## 4. Summary of asymptotic observations in 1-D

The general picture that has emerged is that, for the main types of radial functions considered here, there is always an exponential decay for the leading coefficients. In the RBF cases for which $h(\xi)$ has branch points at $\xi = 0$ and $\xi = 2\pi$ (which also includes TPS), there will also be algebraic terms, which then will come to dominate for high values of $k$. Table 2 summarizes the different rates that arise for the types of radial functions introduced in Table 1.

The algebraic trend, if present at all, is noticeable only after the coefficients have decreased by several orders of magnitude. Furthermore, for decreasing $\varepsilon$, it gets progressively more insignificant in view of the rapid growth of the coefficient for the leading exponential term. From a computational point of view, the rapid growth of all the coefficients poses less of a problem than one might fear. Because of the nature of floating point arithmetic, uniform scalings will not generally lead to any loss of computational accuracy. The exponential rate for MN and TPS becomes less favorable when $j$ increases. This forces for these radial functions a trade-off with accuracy, which generally gets better with increasing $j$.

The cases when $\phi(r)$ is an entire function (GA and BSL) become particularly bad when $\varepsilon \to 0$. For GA, the decay is of the form $O(e^{-\varepsilon^2 k})$ as opposed to $O(e^{-const\cdot\,\varepsilon k})$, and it is essentially lost altogether for BSL when $\varepsilon < \pi$.

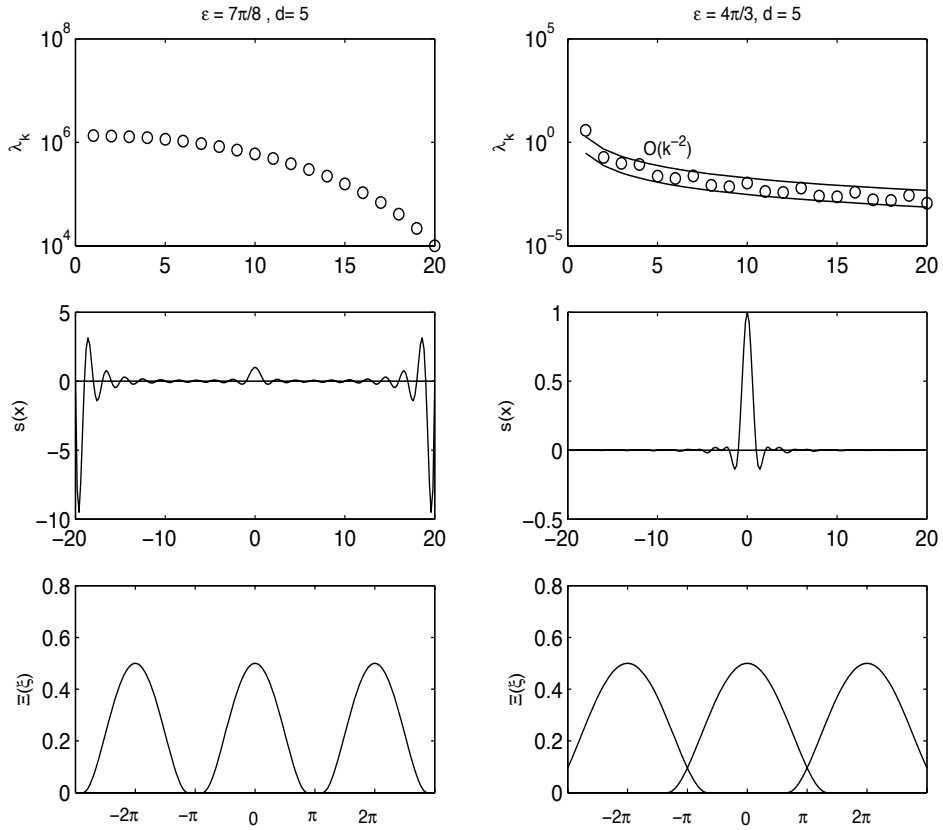


FIG. 6. First row: decay of $\lambda_k$. Notice the difference in vertical scale between the left and right figures. Second row: the interpolant $s(x)$. Third row: the $j = 0, \pm$ terms of the Poisson sum for the indicated value of $\varepsilon$ and $d$. Left column: $\varepsilon = \frac{7}{8}\pi < \pi$; right column: $\varepsilon = \frac{4}{3}\pi > \pi$.

| Type of radial function | | Exponential rate | Algebraic rate |
|---|---|---|---|
| **Piecewise smooth** | | | |
| MN | $j=1$ | $(-1)^k\,5.20\,e^{-1.32k}$ | N/A |
| | $j=2$ | $(-1)^{k+1}\,1.38\,e^{-0.843k}$ | N/A |
| | $j=3$ | $(-1)^k\,0.224\,e^{-0.625k}$ | N/A |
| | $j=4$ | $(-1)^{k+1}\,0.0235\,e^{-0.498k}$ | N/A |
| TPS | $j=1$ | $(-1)^k\,5.30\,e^{-1.81k}$ | $\frac{3}{\pi^2k^4}$ |
| | $j=2$ | $(-1)^{k+1}\,1.81\,e^{-1.02k}$ | $\frac{5}{\pi^2k^6}$ |
| | $j=3$ | $(-1)^k\,0.377\,e^{-0.717k}$ | $\frac{7}{\pi^2k^8}$ |
| | $j=4$ | $(-1)^{k+1}\,0.0486\,e^{-0.554k}$ | $\frac{9}{\pi^2k^{10}}$ |
| **Infinitely smooth** | | | |
| MQ | $\varepsilon=1$ | $(-1)^{k+1}\,17.3\,e^{-1.04k}$ | $-\frac{3}{k^5}$ |
| | $\varepsilon=\frac{1}{10}$ | $(-1)^{k+1}\,1.46\times10^{13}\,e^{-0.150k}$ | $-\frac{3000}{k^5}$ |
| | $\varepsilon\to0$ | $(-1)^{k+1}\,\frac{\pi\sqrt{\varepsilon}}{2^{3/2}}\,e^{\frac{\pi}{\varepsilon}}\,e^{-\frac{\pi}{2}\varepsilon k}$ | $-\frac{3}{\varepsilon^3k^5}$ |
| IQ | $\varepsilon=1$ | $(-1)^{k+1}\,3.68\,e^{-1.57k}$ | $-\frac{1}{\pi^2k^2}$ |
| | $\varepsilon\to0$ | $(-1)^{k+1}\,\frac{\varepsilon^2}{2\pi}\,e^{\frac{\pi}{\varepsilon}}\,e^{-\frac{\pi}{2}\varepsilon k}$ | $-\frac{1}{\pi^2k^2}$ |
| IMQ | $\varepsilon=1$ | $(-1)^{k+1}7.82e^{-1.38k}$ | $\frac{-0.922}{4k(\log k)^2+0.927k\log k+9.92k}$ |
| GA | $\varepsilon^2k>>1$ | $(-1)^k\,\frac{\varepsilon^3}{\pi^{3/2}}\,e^{\frac{\pi^2}{4\varepsilon^2}}\,e^{-\varepsilon^2k}$ | N/A |
| SH | $\varepsilon k>>1$ | $(-1)^k\,\frac{\varepsilon^2}{2\pi}\,e^{\frac{\pi^2}{2\varepsilon}}\,e^{-\varepsilon k}$ | N/A |

Table 2. Leading order exponential and algebraic cardinal coefficient decay rates in 1-D for some different radial functions

## 5. Analysis and observations in 2-D and higher

In the case of GA, we can again find a closed form solution for the cardinal expansion coefficients in any number of dimensions. For the other RBFs, we limit ourselves to 2-D and relate the numerically observed decay rates to characteristics of the 2-D Fourier transform.

### 5.1 *GA*

With $\lambda_k$ chosen according to (2.11), it holds that

$$\sum_{k=-\infty}^{\infty} \lambda_k e^{-\varepsilon^2(k-m)^2} = \begin{cases} 1, & \text{if } m = 0; \\ 0, & \text{if } m = 1. \end{cases}$$

Therefore, in $n$ dimensions,

$$\begin{aligned} \sum_{k_1=\infty}^{\infty} \cdots \sum_{k_n=-\infty}^{\infty} (\lambda_{k_1} \cdot \ldots \cdot \lambda_{k_n}) e^{-\varepsilon^2[(k_1-m_1)^2+\ldots+(k_n-m_n)^2]} \\ = \left( \sum_{k_1=-\infty}^{\infty} \lambda_{k_1} e^{-\varepsilon^2(k_1-m_1)^2} \right) \cdot \ldots \cdot \left( \sum_{k_n=-\infty}^{\infty} \lambda_{k_n} e^{-\varepsilon^2(k_n-m_n)^2} \right) \\ = \begin{cases} 1, & \text{if } m_1 = m_2 = \cdots = m_n = 0; \\ 0, & \text{otherwise,} \end{cases} \end{aligned}$$

and we have obtained $\lambda_{k_1,k_2,\ldots,k_n} = \lambda_{k_1} \cdot \lambda_{k_2} \cdot \ldots \cdot \lambda_{k_n}$. This is an exact formula for the RBF coefficients in $n$-D. Notice that they are simply a product of the 1-D coefficients along each of the $n$ dimensions, immediately confirming the pyramid shaped angular dependence seen later on in the GA case of Figure 10. The lack of a simple generalization of Cauchy's Theorem to functions of several complex variables makes the type of analysis we used in 1-D difficult to carry over. However, numerical computation of the cardinal coefficients is again straightforward (noting that the integrals in (2.5) can be rapidly approximated by FFTs).

We will return to the GA RBF in Section 5.3.

### 5.2 *Cubic RBF*

Figure 7 shows numerically computed values for $\log|\lambda_{k_1,k_2}|$ near the origin in the $k_1,k_2$-plane.
The coefficients decay exponentially fast for small $k$, with different rates depending on the direction in the $k_1,k_2$-plane, as shown in Figure 8.

Each of the subplots in Figure 8 is similar to the 1-D case in the left subplot of Figure 3 in that there are two decay regimes. While we have not been able to find any closed form analytic expressions for the direction dependent exponential decay regime, the algebraic decay regime that dominates for large $k$, is shown below to be

$$\lambda_{k_1,k_2} \approx -\left(\frac{5}{2\pi}\right)^2 \frac{1}{k^7} \tag{5.1}$$

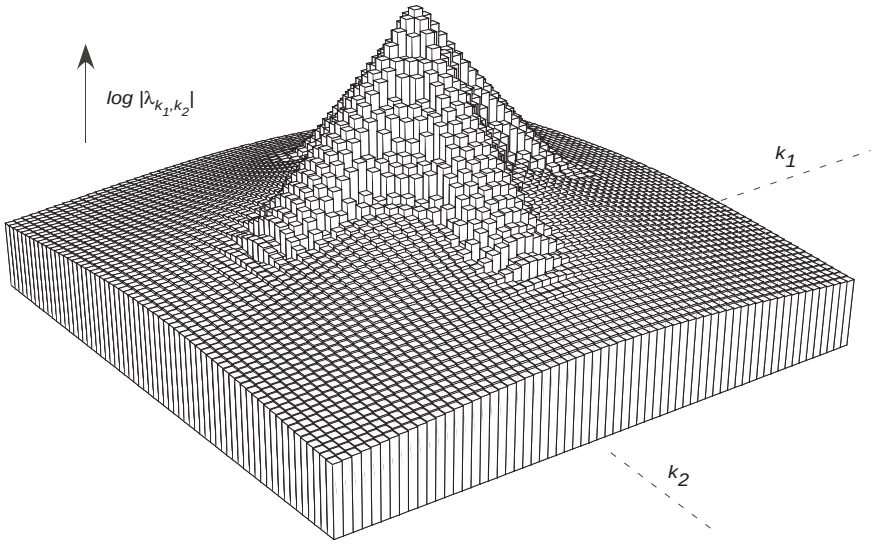


FIG. 7. Display of $\log|\lambda_{k_1,k_2}|$ for cubic RBFs in 2-D centered at $(k_1,k_2)=(0,0)$.

where $k=\sqrt{k_1^2+k_2^2}$. Figure 9 shows the six subplots from Figure 8 superposed on each other, together with (dashed) the curve corresponding to (5.1). The agreement is excellent. A different method of arriving at the algebraic decay rates (by repeated integration-by-parts) is given in Section 4.2.4 of Buhmann (2003).

5.2.1 *Proof of (5.1)* The generalized 2-D Fourier transform for cubics is $\widehat{\phi}(\rho)=\frac{9}{\rho^5}$ (cf. Table 1). The denominator $g(\xi_1,\xi_2)=\sum_{j_1=-\infty}^{\infty}\sum_{j_2=-\infty}^{\infty}\widehat{\phi}(\|\underline{\xi}+2\pi\underline{j}\|)$ in (2.5) will therefore go to infinity in this manner at the origin and at each $2\pi$-periodic repetition of the origin. The function $h(\xi_1,\xi_2)=\frac{1}{g(\xi_1,\xi_2)}$ will, at the origin (and at its periodic repetitions), take the form

$$h(\xi_1,\xi_2)=\frac{1}{9}(\xi_1^2+\xi_2^2)^{5/2}+\ \{\text{a smooth function}\}. \tag{5.2}$$

We note that the cardinal expansion coefficients are proportional to the Fourier series coefficients of the doubly $2\pi$-periodic function $h(\xi_1,\xi_2)$. To see what effect these irregularities have on the coefficient decay rate, we consider also:

**Poisson's summation formula in 2-D:** If a function $f(\xi_1,\xi_2)$ has the Fourier transform $\widehat{f}(\omega_1,\omega_2)$, then the doubly periodic function

$$\sum_{j_1=-\infty}^{\infty}\sum_{j_2=-\infty}^{\infty} f(\xi_1+2\pi j_1,\xi_2+2\pi j_2)$$

has the Fourier series

$$\frac{1}{2\pi}\sum_{k_1=-\infty}^{\infty}\sum_{k_2=-\infty}^{\infty}\widehat{f}(k_1,k_2)\,e^{i(k_1\xi_1+k_2\xi_2)}.$$

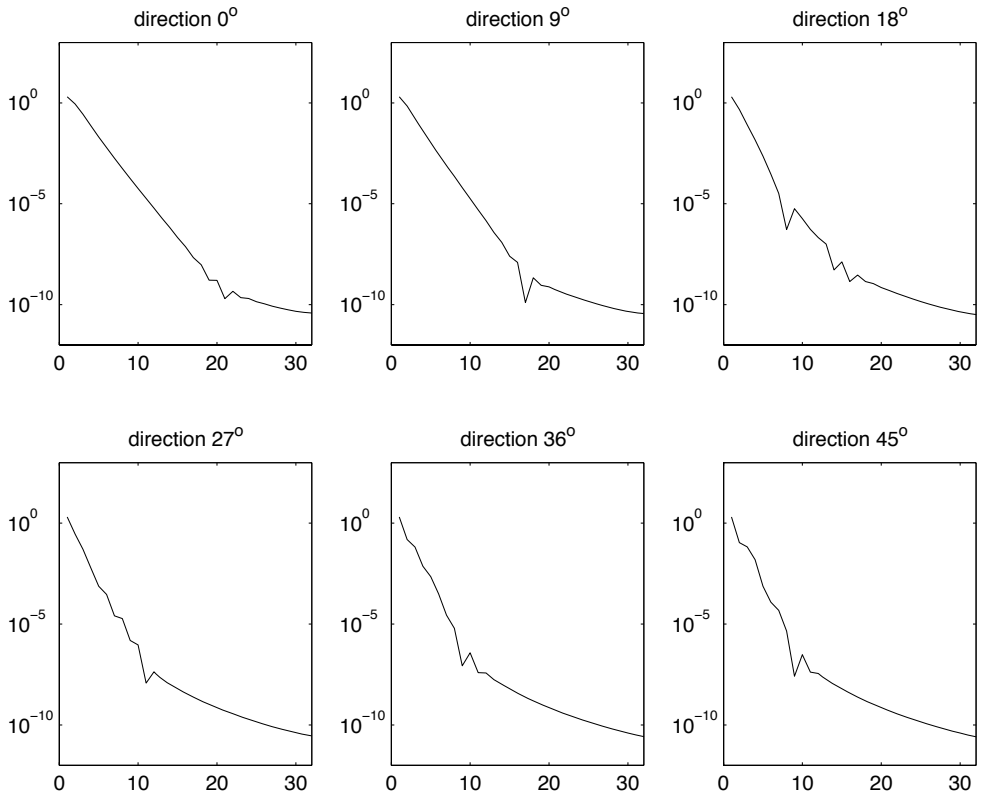


FIG. 8. Log-linear plots of the decay rates of the expansion coefficients in different directions in the $k_1, k_2$-plane. Vertical direction shows $\log|\lambda_{k_1,k_2}|$, horizontal $\sqrt{k_1^2+k_2^2}$.

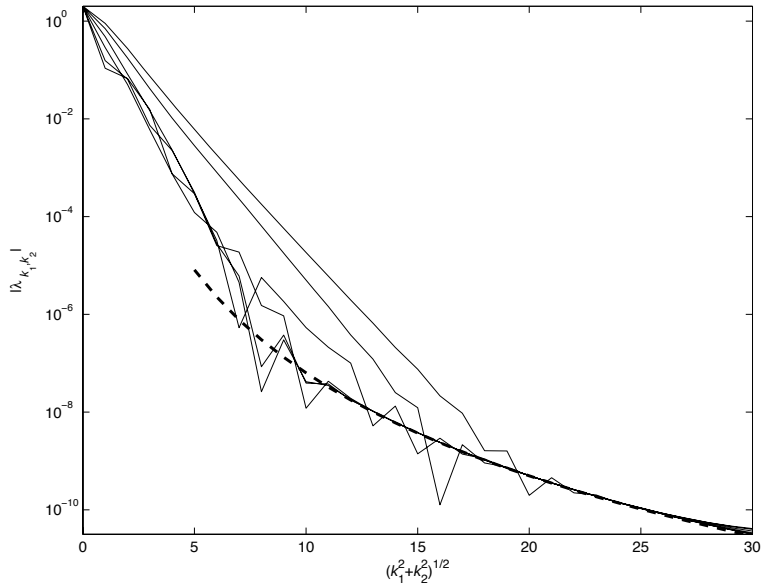


FIG. 9. Decay rates of $|\lambda_{k_1,k_2}|$ in different directions in the $k_1,k_2$-plane, with the result from (5.1) superimposed as a dashed curve.

To use this result effectively, we first apply the Laplacian operator $\Delta = \frac{\partial^2}{\partial\xi_1^2} + \frac{\partial^2}{\partial\xi_2^2}$ several times (e.g. four times; the exact number does not influence the result) to $h(\xi_1,\xi_2)$, leading to a function which is dominated by the singularities:

$$\Delta^4 h(\xi_1,\xi_2) = 25(\xi_1^2+\xi_2^2)^{-3/2} + \{\text{a smooth function}\}.$$

Its Fourier transform at the integer lattice points, $-25(k_1^2+k_2^2)^{1/2}$, should equal the Fourier coefficients of the function $h(\xi_1,\xi_2)$, with the Laplacian applied four times, i.e. $(k_1^2+k_2^2)^4\lambda_{k_1,k_2}$. This gives (5.1).

### 5.3 *TPS, GA, AND SH*

In contrast with the situation for the cubic RBF (Section 5.2.1), the functions $g(\xi_1,\xi_2)$ for the TPS, GA, and SH RBFs are infinitely smooth at the origin and at their $2\pi$-periodic repetitions (cf. Table 1). Therefore the decay of the coefficients never becomes algebraic, as can be seen in Figure 10. It should be noted that the type of angular symmetry observed in the GA case is directly due to the grid layout, e.g. a rectalinear (Cartesian) grid layout produces four fold symmetry, a hexagonal grid layout will produce six fold symmetry.

### 5.4 *MQ, IMQ, and IQ*

The situation in these cases is analogous to that of the cubic RBF since the 2-D generalized Fourier transforms of these RBFs each go to infinity as the origin ($\rho = 0$), but do this in such a way that their inverses are non-smooth across $\rho = 0$ (cf. Table 1). That is, we expect the decay of the coefficients to become algebraic after an initial exponential decay regime. Figure 10 shows that this is indeed the case.

Following a procedure similar to that described in Section 5.2.1, it has been found that the algebraic decay for MQ goes to leading order as $\left(\frac{3}{2\pi}\right)^2 \frac{1}{k^5}$, and for IMQ as $\left(\frac{1}{2\pi}\right)^2 \frac{1}{k^3}$. The decay for IQ is more complicated, involving logarithmic components.

## 6. Summary of observations for RBF cardinal coefficient decay

Previous literature on the topic has left many questions unanswered: To what extent are the RBF cardinal coefficients, $\lambda_k$, localized? If there is a localization attribute to the coefficients, what is the behavior of the coefficients as $|k| = \sqrt{k_1^2 + k_2^2}$ increases from small to large? What happens in higher dimensions? Is the decay rate of $\lambda_k$ only dependent on radial distances or do angular dependencies come in? In this study, we have addressed these and other questions through both analytical (primarily contour integration in the complex plane) and numerical techniques. In addition, we have also introduced a seldom (if ever) used radial function $\mathrm{sech}(\varepsilon r)$, giving a proof of the non-singularity of its interpolation matrix in $n$ dimensions for scattered data. The observations that have emerged for the RBFs considered in this paper are summarized below.

1. For all RBFs in 1-D and 2-D, except Bessel RBFs (for which the Poisson sum can be zero due to the compactness of its Fourier transform), the leading order behavior of the expansion coefficients for small $|k|$ is exponential decay.

2. However, the leading order behavior of the coefficients can change from exponential decay (as noted in (1)) to algebraic decay as $|k|$ increases, exhibiting two different decay regimes in this limit. In particular, this will occur when $1/\widehat{\phi}(\rho)$ is non-smooth across the origin. Such cases include MN in even dimensions, TPS in odd dimensions, MQ, IMQ, and IQ.

3. For those RBFs that do exhibit two different decay regimes for increasing $k$ and do not grow rapidly far out, which would exclude TPS, the exponential decay behavior of the coefficients for small $k$ determines the localization property of the RBF interpolant. When the leading order behavior becomes algebraically decaying, $\lambda_k$ has typically decreased by many orders of magnitude (e.g. for MQ in 1-D, with $\varepsilon = 1$, $\lambda_k \approx O(10^{-6})$, contributing less than 1% to the value of the interpolant at the cardinal point.

4. For 2-D, in the regime of exponential decay, (i.e. for small $|k|$, $|k| = \sqrt{k_1^2 + k_2^2}$), the behavior of the coefficients always has an angular dependence in the $k_1$, $k_2$ plane. If algebraic decay comes to dominate the leading order behavior as $k$ increases, the dependence will then become purely radial.

It may also be convenient to have available some heuristic guidelines with regard to RBFs in general that allow for quick assessment of the cardinal coefficient decay rate. Hence, we note the following in 1-D:

1. If $\phi(r)$ decays exponentially fast to zero for increasing $r$ (e.g. GA and SH), $\widehat{\phi}(\xi)$ will be analytic in a strip around the $\xi$-axis, implying that the decay of $\lambda_k$ will be of exponential form for all $k$ (i.e. will not be overtaken by any slower algebraic rate for large $k$).

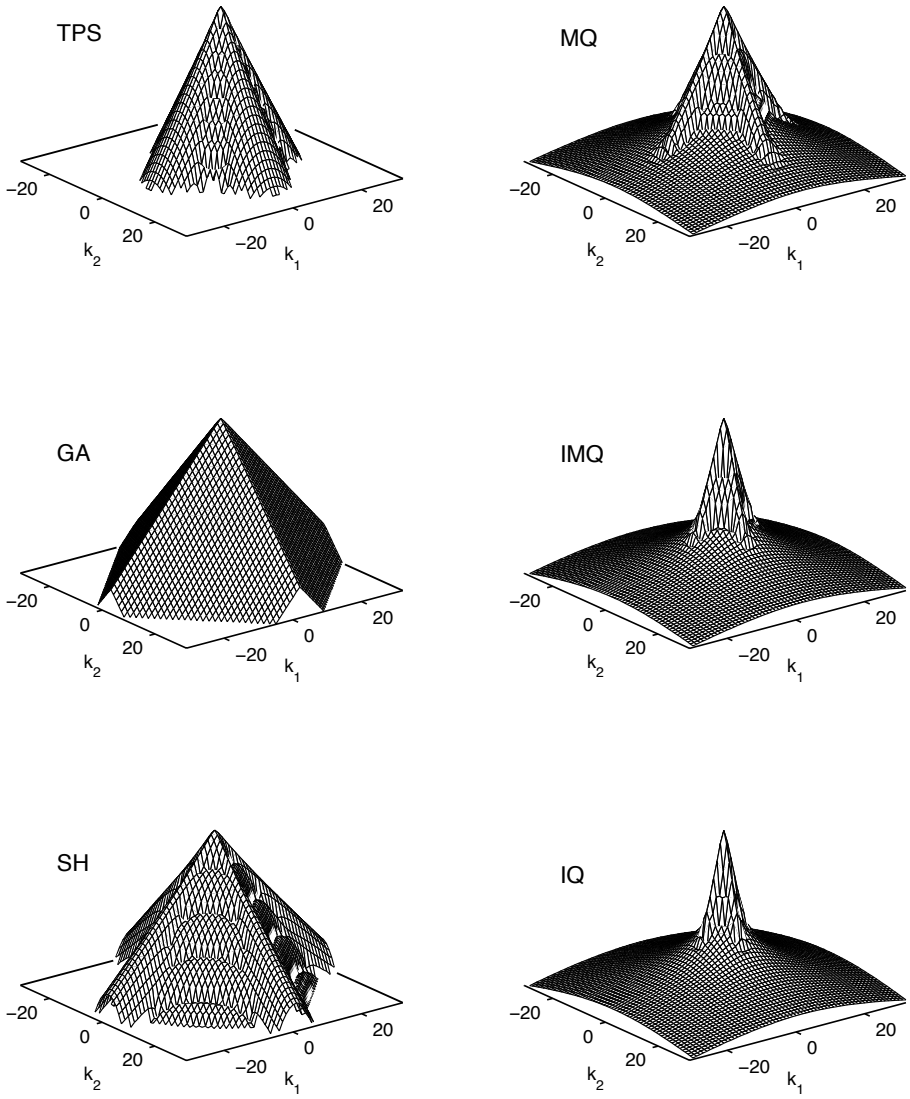


FIG. 10. Decay of expansion coefficients for 2D cardinal data for the TPS, MQ, GA, IMQ, SH, and IQ RBFs displayed in the same log-linear format used in Figure 7. Note that the TPS, GA, and SH RBFs manifest an exponential decay regime only.

2. If $\phi(r)$ is of the form $\phi(r) = |r|^{2j+1}$, $j = 0, 1, \ldots$ (MN, or a linear combination of such), the decay will again be purely exponential.

3. If $\phi(r)$ is analytic and grows for increasing $r$ like $|r|^{\alpha}$ (e.g. GMQ), there will be an algebraic decay rate present, which is particularly small whenever $\alpha$ is an odd positive integer (e.g. MQ).

4. If $\phi(r)$ is analytic in a finite width strip $|\mathrm{Im}\, r| \leqslant a(\varepsilon)$ around the real axis, the exponential part of the decay will typically (e.g. GMQ, SH) be of the form $O\left(e^{-k\pi/(2a(\varepsilon))}\right)$ when $\varepsilon \to 0$.

**Acknowledgement** The National Center for Atmospheric Research is sponsored by the National Science Foundation. Dr. Bengt Fornberg would like to acknowledge the support of NSF grants DMS-0309803 and DMS-0611681. Dr. Natasha Flyer would like to acknowledge the support of NSF grant ATM-0620100. Ms. Cécile Piret was supported under NSF grant DMS-0309803.

## A. Non-singularity of the RBF interpolant (in $n$ dimensions, scattered data) in the SH case ($\phi(r) =$ **sech**$(\varepsilon r)$)

By the Schoenberg interpolation theorem (Cheney & Light (2000), p. 101), the result follows if we can show that $\mathrm{sech}(\sqrt{x})$ is a completely monotone function. By the Bernstein-Widder theorem (Cheney & Light (2000), p. 95) this will be the case if and only if the inverse Laplace transform $\gamma(s)$ of $\mathrm{sech}(\sqrt{x})$ is non-negative for $0 < s < \infty$. From the expansion $\mathrm{sech}(\sqrt{x}) = 2(e^{-\sqrt{x}} - e^{-3\sqrt{x}} + e^{-5\sqrt{x}} - + \ldots)$ follows

$$\gamma(s) = \frac{1}{\sqrt{\pi} s^{3/2}} \left( e^{-\frac{1}{4s}} - 3e^{-\frac{9}{4s}} + 5e^{-\frac{25}{4s}} - 7e^{-\frac{49}{4s}} + - \ldots \right).$$

This can be written as $\gamma(s) = \frac{1}{\sqrt{\pi} s^{3/2}} \xi(\frac{1}{4\pi s})$ using the $\xi$-function defined in (3.5) It remains only to show that $\xi(s) > 0$ for $0 < s < \infty$. This result is trivial for $s \geqslant 1$ (since the positive terms in (3.5) for $j = 0$ and $j = -1$ then dominate all remaining terms), and it then holds also for $0 < s \leqslant 1$ because of (3.4).

## B. Asymptotic analysis for GMQ in 1-D

The generalized multiquadric RBF has the form $\phi(r; \beta, \varepsilon) = (1 + \varepsilon^2 r^2)^{\beta}$. Its Fourier transform is given by

$$\widehat{\phi}(\rho; \beta, \varepsilon) = \frac{2^{\beta+1}}{\Gamma(-\beta)\varepsilon} \left( \frac{K_{\beta+1/2}(\frac{|\rho|}{\varepsilon})}{(\frac{|\rho|}{\varepsilon})^{\beta+\frac{1}{2}}} \right).$$

Note that $\widehat{\phi}$ for nonnegative integer values of $\beta$ is singular, as also indicated by Figure 5. By equation (2.3),

$$\lambda_k = \frac{\varepsilon \Gamma(-\beta)}{2^{\beta+\frac{5}{2}} \pi^{\frac{3}{2}}} \int_0^{2\pi} \frac{e^{ik\xi} d\xi}{\sum_{j=-\infty}^{\infty} \frac{K_{\beta+1/2}(\frac{|\xi+2\pi j|}{\varepsilon})}{(\frac{|\xi+2\pi j|}{\varepsilon})^{\beta+\frac{1}{2}}}}. \tag{B.1}$$

We find the analog of (3.1) to be

$$h(\xi;\beta,\varepsilon) = \frac{1}{\sum\limits_{j=0}^{\infty} \frac{K_{\beta+1/2}(\frac{2\pi j+\xi}{\varepsilon})}{(\frac{2\pi j+\xi}{\varepsilon})^{\beta+\frac{1}{2}}} + \sum\limits_{j=1}^{\infty} \frac{K_{\beta+1/2}(\frac{2\pi j-\xi}{\varepsilon})}{(\frac{2\pi j-\xi}{\varepsilon})^{\beta+\frac{1}{2}}}}.$$

### B.1 *Exponential decay*

The poles of $h(\xi;\beta,\varepsilon)$ are located on the line $\xi = \pi + it$. On this line, the value of $h(\xi;\beta,\varepsilon)$ is purely real. In order to find their contribution to the integral, it is necessary to find the locations of the poles as well as the residues associated with them. Because we are looking for the leading terms, it is sufficient to find the location of the first pole of $h(\xi;\beta,\varepsilon)$ only. We then look for the first zero of $g(\xi;\beta,\varepsilon) = \frac{1}{h(\xi;\beta,\varepsilon)}$ on $\xi = \pi + it$. Due to the rapid decay of the $K$ Bessel function, it is sufficient to use only the center term of the sum in $h(\xi;\beta,\varepsilon)$. For small enough $\varepsilon$, the $K$ Bessel function can be approximated by formula 9.7.2 of Abramowitz & Stegun (1981). For $|\beta| < \frac{5}{2}$ the first two terms are adequate: $K_\nu(z) \approx \sqrt{\frac{\pi}{2z}}\, e^{-z}\left(1 + \frac{4\nu^2-1}{8z}\right)$. We get

$$\begin{aligned} g(\pi+it;\beta,\varepsilon) &\approx \frac{K_{\beta+1/2}(\frac{\pi+it}{\varepsilon})}{(\frac{\pi+it}{\varepsilon})^{\beta+\frac{1}{2}}} \\ &\approx \frac{e^{-\frac{\pi+it}{\varepsilon}}\sqrt{\frac{\pi}{2}}\left(\frac{\pi+it}{\varepsilon}\right)^{-\beta}\varepsilon(2\pi+2it+\beta(1+\beta)\varepsilon)}{2(\pi+it)^2} \end{aligned}$$

The zero of $g(\pi+it;\beta,\varepsilon)$ can therefore be found by solving

$$(\beta+2)\tan^{-1}\left(\frac{t}{\pi}\right) + \frac{t}{\varepsilon} + \tan^{-1}\left(\frac{-2t}{2\pi+\beta(1+\beta)\varepsilon}\right) = \frac{\pi}{2} + \pi\sigma,$$

where $\sigma$ is an integer. Setting $\sigma = 0$ and approximating $\tan^{-1}(z) \approx z$, we get $t_{pole} \approx \frac{\pi}{2\left(\frac{2+\beta}{\pi} + \frac{1}{\varepsilon} - \frac{2}{2\pi+\beta(1+\beta)\varepsilon}\right)}$.

Therefore, $\lambda_k$, for relatively small values of $k$, can be approximated as

$$\begin{aligned} \lambda_k &\approx \frac{\varepsilon\,\Gamma(-\beta)}{2^{\beta+\frac{5}{2}}\pi^{\frac{3}{2}}}(2\pi i \,\mathrm{Res}(h(z)e^{ikz}, z = \pi + it_{pole})) \\ &= (-1)^{k+1}\frac{\varepsilon\,\Gamma(-\beta)}{2^{\beta+\frac{3}{2}}\sqrt{\pi}}\,\frac{1}{\frac{d}{dt}g(\pi+it)_{t=t_{pole}}}\,e^{-kt_{pole}}. \end{aligned} \tag{B.2}$$

### B.2 *Algebraic decay*

We again approximate $h(\xi;\beta,\varepsilon)$ by means of just one term of the Poisson sum:

$$h(\xi;\beta,\varepsilon) \approx f(\xi;\beta,\varepsilon) \equiv \frac{\left(\frac{\xi}{\varepsilon}\right)^{\beta+\frac{1}{2}}}{K_{\beta+\frac{1}{2}}\left(\frac{\xi}{\varepsilon}\right)} \tag{B.3}$$

#### B.2.1 *Positive $\beta$*

$\beta$ A HALF-INTEGER When $\beta = \mu + 1/2$, with $\mu$ a non-negative integer, the leading singularity looks like $\frac{(-1)^{\mu+1}(\frac{\xi}{\varepsilon})^{4\mu+4}\log(\frac{\xi}{\varepsilon})}{(\mu!)^2(\mu+1)!2^{3\mu+1}}$. To compute the contribution of the branch point singularity to the integral in (B.1), we start by noting that $h(\xi;\beta,\varepsilon)$ is purely real along both of the straight lines $\operatorname{Im}\xi = 0$ and $\operatorname{Re}\xi = \pi$. Then, by the Schwarz reflection principle, the contour integral, which should be taken along sections $\{1\}$ and $\{2\}$ in Figure 2 (and also along a connection path high up), can just as well be taken along sections $\{1\}$ and $\{4\}$, leading to a simple treatment of the branch issue. We therefore get

$$\lambda_k \approx \frac{\varepsilon\Gamma(-\mu-1/2)}{(2\pi)^{3/2}2^{\mu+3/2}} \frac{(-1)^{\mu+1}i\pi}{(\mu!)^2(\mu+1)!2^{3\mu+1}} \int_0^{i\infty} \left(\frac{\xi}{\varepsilon}\right)^{4\mu+4} e^{ik\xi} d\xi. \tag{B.4}$$

Setting $\xi = it$ and integrating leads to

$$\lambda_k = \frac{\Gamma(-\beta)(4\beta+2)!}{2^{4\beta+2}\sqrt{\pi}\left((\beta-\frac{1}{2})!\right)^2(\beta+\frac{1}{2})!\,\varepsilon^{4\beta+1}} \frac{1}{k^{4\beta+3}}. \tag{B.5}$$

$\beta$ NOT A HALF-INTEGER In this case the branch point at the origin is algebraic (instead of logarithmic):

$$f(\xi;\beta,\varepsilon) \approx \frac{\xi^{1+2\beta}\cos(\pi\beta)\Gamma(\frac{1}{2}-\beta)}{2^{\beta-\frac{1}{2}}\pi\varepsilon^{2\beta+1}}$$

Computing the contour integral along sections $\{1\}$ and $\{4\}$ in Figure 2 leads to

$$\lambda_k \approx \frac{(2\beta+1)\cot(\pi\beta)}{2\pi\varepsilon^{2\beta}} \frac{1}{k^{2(\beta+1)}} \tag{B.6}$$

B.2.2 *Negative $\beta$*

$\beta > -1$ Referring to equation (B.3), we make the approximation that, for small $\xi$,

$$K_{\frac{1}{2}+\beta}\left(\frac{\xi}{\varepsilon}\right) \approx -\gamma - \log\left(\frac{\xi}{2\varepsilon}\right).$$

This yields

$$f(\xi;\beta,\varepsilon) \approx -\frac{\Gamma(-\beta)\varepsilon^{\frac{1}{2}-\beta}\xi^{\frac{1}{2}+\beta}}{2^{\beta+1}\left[\gamma+\log\left(\frac{\xi}{2\varepsilon}\right)\right]}.$$

Now the equivalent of equation (B.4) will contain logarithms. We make the change of variables $z = \log\xi$ and then apply Laplace's method for integrals with movable maxima as described in Ablowitz & Fokas (2003) and Bender & Orszag (1999). The result is that

$$\lambda_k \approx -\frac{(3+2\beta)\varepsilon^{\frac{1}{2}-\beta}\Gamma(-\beta)\left[\pi\cos\left(\frac{\pi}{4}(1+2\beta)\right) - 2\left(\gamma+\log\left(\frac{3+2\beta}{4k\varepsilon}\right)\right)\sin\left(\frac{\pi}{4}(1+2\beta)\right)\right]}{2^{1+\beta}e^{\frac{3}{2}+\beta}\left(\frac{3}{2}+\beta\right)^{-\beta}\pi\left(4\gamma^2+\pi^2+8\gamma\log\left(\frac{3+2\beta}{4k\varepsilon}\right)+4\log^2\left(\frac{3+2\beta}{4k\varepsilon}\right)\right)} \frac{1}{k^{\frac{3}{2}+\beta}}. \tag{B.7}$$

This approximation works well for values of $\beta$ near $-\frac{1}{2}$. Degradation of the approximation near the ends of the interval $(-1,0)$ is due to the lack of $\beta$ dependence in the approximation for the Bessel $K$ function. Adding more terms to the Bessel $K$ approximation solves this problem at the cost of a much more complicated expression for $\lambda_k$.

$\beta = -1$ In this case we have

$$\widehat{\phi}(\rho;\varepsilon) = \frac{\sqrt{\pi}}{\sqrt{2}\,\varepsilon}\, e^{-\frac{|\rho|}{\varepsilon}}$$

and

$$f(\xi;\varepsilon) = \frac{\sqrt{2}\,\varepsilon}{\sqrt{\pi}} e^{\frac{\rho}{\varepsilon}}.$$

Integrating as before yields

$$\lambda_k \approx -\frac{1}{\pi^2 k^2}. \tag{B.8}$$

Numerical tests have confirmed that the leading algebraic decay does not depend on $\varepsilon$.

$\beta < -1$ We note now that $K_{-\nu}(z) = K_\nu(z)$. Then, when $\beta < 0$, it must be true that $K_{\beta+1/2}(z) = K_{1/2+(-1-\beta)}(z)$. Let $\hat{\beta} = -1-\beta > -1$. Then,

$$\begin{aligned} \frac{(\frac{\xi}{\varepsilon})^{\beta+1/2}}{K_{\beta+1/2}(\frac{\xi}{\varepsilon})} &= \left(\frac{\xi}{\varepsilon}\right)^{1+2\beta} \frac{(\frac{\xi}{\varepsilon})^{\hat{\beta}+1/2}}{K_{\hat{\beta}+1/2}(\frac{\xi}{\varepsilon})} \\ &= \left(\frac{\xi}{\varepsilon}\right)^{1+2\beta} f(\xi;\hat{\beta},\varepsilon) \end{aligned}$$

where $f(\xi;\hat{\beta},\varepsilon)$ is the approximation of $h(\xi;\hat{\beta},\varepsilon)$, defined for $\hat{\beta} = -1-\beta > -1$. Taking the two-term approximation

$$f(\xi;\hat{\beta},\varepsilon) \approx \frac{\cos(\pi\beta)\Gamma(\frac{1}{2}-\hat{\beta})}{2^{3\hat{\beta}+\frac{1}{2}}\pi\,\Gamma(\frac{3}{2}+\hat{\beta})} \left(\frac{\xi}{\varepsilon}\right)^{1+2\hat{\beta}} \left( \left(\frac{\xi}{\varepsilon}\right)^{1+2\hat{\beta}} \Gamma(\tfrac{1}{2}-\hat{\beta}) + 2^{1+2\hat{\beta}}\,\Gamma(\tfrac{3}{2}+\hat{\beta}) \right)$$

and computing the contour integral as before gives

$$\lambda_k \approx \frac{(\cos(\pi\beta)\Gamma(-\beta)\Gamma(\frac{3}{2}+\beta))^2}{\pi^3\,\varepsilon^{-2\beta-2}}\,\frac{1}{k^{-2\beta}}. \tag{B.9}$$

## REFERENCES

ABLOWITZ, M.J. & FOKAS, A.S. (2003) *Complex Variables, 2nd Ed.*, Cambridge University Press, Chapter 6.
ABRAMOWITZ, M. & STEGUN, I.A., (1981) *Handbook of Mathematical Functions*, Dover Publications.
ARSAC, J. (1966) *Fourier Transforms and the Theory of Distributions*, Prentice Hall, 1966.

BENDER, C.M. AND ORSZAG, S.A. (1999) *Advanced Mathematical Methods for Scientists and Engineers*, Springer-Verlag, Chapter 6.

BUHMANN, M. D. (1988) *Multivariate interpolation with radial basis functions*, Technical Report DAMPT 1988/NA8, University of Cambridge.

BUHMANN, M. D. (1993) On quasi-interpolation with radial basis functions, *J. Approx. Theo.,* **72**, 103–230.

BUHMANN, M. D. (2003) *Radial Basis Functions*, Cambridge University Press.

BUHMANN, M. D. & POWELL, M.J.D. (1990) Radial basis function interpolation on an infinite regular grid, In: J. C. MASON AND M. G. COX, eds. *Algorithms for Approximation II*, Chapman and Hall, 146–169.

CHENEY, W. & LIGHT, W. (2000) *A Course in Approximation Theory*, Brooks/Cole Publishing Company.

DRISCOLL, T.A. & FORNBERG, B. (2002) Interpolation in the limit of increasingly flat radial basis functions, *Comp. Math. Appl.,* **43**, 413–422.

FAUL, A.C. & POWELL, M. J. D. (2000) Krylov subspace methods for radial function interpolation, In: D. F. GRIFFITHS & G. A. WATSON, eds. *Numerical Analysis 1999*, Chapman and Hall, 115–141.

FLYER, N. (2006) Exact polynomial reproduction for oscillatory radial basis functions on infinite lattices, *Comp. Math. Appl.* **51**, 1199–1208.

FORNBERG, B. (1996) *A Practical Guide to Pseudospectral Methods*, Cambridge University Press, 1996.

FORNBERG, B., DRISCOLL, T.A., WRIGHT, G. AND CHARLES, R.(2002) Observations on the behavior of radial basis functions near boundaries, *Comp. Math. Appl.* **43**, 473–490.

FORNBERG, B. & FLYER, N. The Gibbs Phenomenon for Radial Basis Functions, In: A. JERRI, ed.*The Gibbs Phenomenon in Various Representations and Applications*, Sampling Publishing, Potsdam, NY, in press.

FORNBERG, B., LARSSON, E. AND WRIGHT, G. (2006) A new class of oscillatory radial basis functions, *Comp. Math. Appl.*, 1209–1222.

FORNBERG, B. & WRIGHT, G., Stable computation of multiquadric interpolants for all values of the shape parameter, *Comp. Math. Appl.,* **48**, 853–867.

FORNBERG, B., WRIGHT, G., & LARSSON, E. (2004) Some observations regarding interpolants in the limit of flat radial basis functions, *Comp. Math. Appl.,* **47**, 37–55.

GNEITING, T. (1997) Normal scale mixtures and dual probability densities, *J. Stat. Comp. Simul.,* **59**, 375–384.

JONES, D.S. (1966) *Generalized Functions*, McGraw-Hill.

LIGHTHILL, M.J. (1958) *Fourier Analysis and Generalized Functions*, Cambridge University Press.